CERN-ACC-NOTE-2019-0055

6 December 2019
sofia.kostoglou@cern.ch

MD4147: 50 Hz harmonics perturbation

S. Kostoglou, D. Alves, G. Arduini, C. Baccigalupi, H. Bartosik,
M. C. Bastos, X. Buffat, J.-P. Burnet, L. R. Carver, R. De Maria,
S. Fartoukh, R. T. Garcia, G. Iadarola, L. Intelisano, T. Levens, O. Michels,
V. Montabonnet, D. Nisbet, J. Olexa, Y. Papaphilippou, M. Pojer,
A. Poyet, M. Soderen, M. Solfaroli, G. Sterbini, H. Thiesen, G. Trad,
N. Triantafyllou, D. Valuch, J. Wenninger
CERN, CH-1211 Geneva, Switzerland

Keywords: 50 Hz harmonics, main bends, external noise, active filters, ADT, MD4147

Summary

Since the beginning of the LHC commissioning, harmonics of 50 Hz have been observed in the beam spectrum. Several observations during the 2018 proton run show that these harmonics are the result of a real beam excitation, rather than an artifact of the instrumentation system. As many of these components reside in the vicinity of the betatron tune, their presence can complicate the tune measurement and tracking during operation and potentially lead to beam losses and emittance growth. This note summarizes the program of the first LHC Machine Development (MD) (Fills 7342 and 7343) dedicated to the investigation of this effect. The aim of this study is to reproduce some of the observations acquired during End-of-Fill experiments and parasitic observations, as well as to simulate the impact of dipolar noise on the beam with controlled ADT excitations.

Contents

1 Introduction

The MD was dedicated to the investigation of the 50 Hz harmonics that have been observed in the beam spectrum [1, 2]. Previous studies have identified two regimes of interest in frequency domain [3–5]: first, a cluster of 50 Hz harmonics extending approximately up to 3.6 kHz (low frequency cluster) and second, a cluster at the location $f_{rev} - f_x$ (high frequency cluster), where f_{rev}, f_x are the revolution (≈ 11.24 kHz) and the betatron frequency, respectively. Both regimes consist of several multiples of 50 Hz that are not sidebands around the tune, an observation that indicates that the effect is dipolar. Figure 1 depicts the horizontal spectrum of Beam 2 at Stable Beams. The spectrum is computed from the average of the bunch-by-bunch position measurements as acquired from the Q7 pickup of the ADTObsBox. The phase evolution of the bunch spectra has been considered in the analysis and a correction is applied to remove the dephasing before combining the bunch-by-bunch measurements. The two clusters are depicted with the blue and orange span, respectively. The maximum amplitude of this perturbation is ≈ 150 nm at top energy.

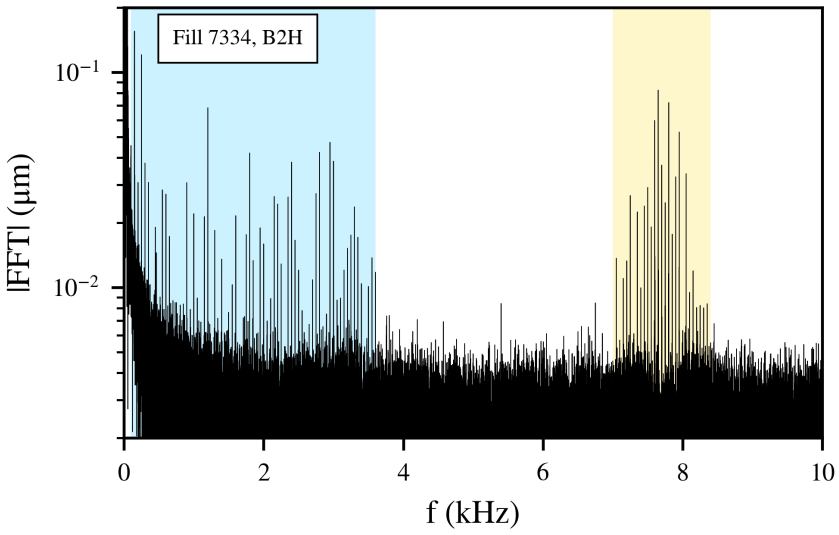

Figure 1: The horizontal spectrum of Beam 2 at Stable beams. The blue and orange span indicates the low and high frequency cluster of 50 Hz harmonics, respectively.

In this context, the main objectives of the MD were:

- The high frequency cluster. To investigate whether these harmonics have an evolution in frequency domain that is similar to the ones of the low frequency cluster, consecutive high-sampling rate measurements were collected during the MD from the Multiband Instability Monitor (MIM) (T. Levens) [6]. The similarities between the two can be identified using the measurements collected parasitically during the MD.
- Active filters. Previous experiments have revealed a correlation between the harmonics of the beam and noise in the power converters of the main dipoles through modifications in the status of the Active filters. The aim of this study is to reproduce these results and to identify the frequencies that are impacted by this modification.

- ADT controlled excitations. The goal of this study is to use the transverse damper to inject dipolar noise on the beam and to reproduce some of the previous observations in a controlled manner. The value of the initial kick for various excitation frequencies is retrieved through an analytical approach based on the beam response (calibrated metric from ADTObsBox [7]). To this end, regular acquisitions from the ADTObsBox were triggered (D. Valuch, M. Soderen). These values are employed to benchmark the results of the simulations in the presence of noise.

- IP1/5 phase scan. Previous experiments (MD 3583 [8]) have shown that a modification of the phase advance between IP1 and 5 at top energy led to distinct changes in the amplitude evolution of the harmonics in the low frequency cluster. Amongst others, this finding provides a definitive indication that the harmonics are the result of a real beam excitation. Figure 2 presents the amplitude evolution of the h=12 harmonic (black) when the phase advance between the two IPs was modified within a range of $\pm$ 20 $^\circ$ (red). The aim of this test is to reproduce these results at injection energy and potentially extract additional information concerning the distribution of the noise in the lattice.

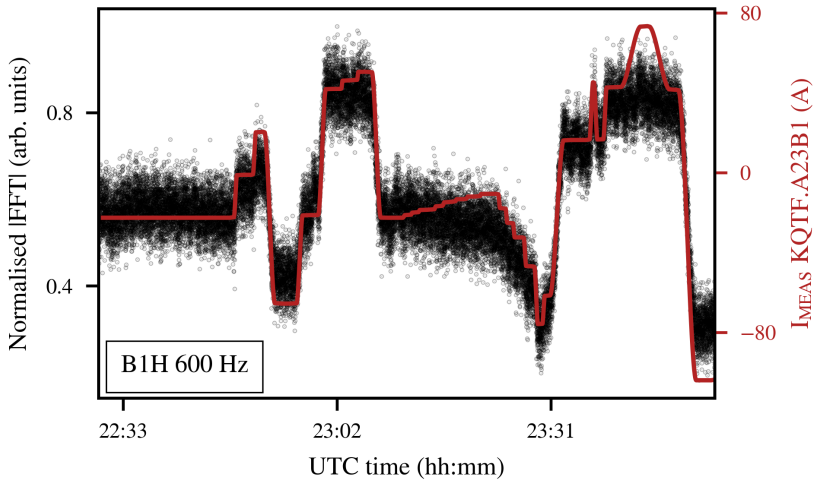

Figure 2: The amplitude evolution of the h=12 harmonic (black) during the change of the phase advance between IP1 and 5. The red line corresponds to the current of one of the quadrupoles used for the phase scan.

2 MD overview

On 25 October 2018, during the MD4 block, a slot of 5 hours was assigned to this MD [9]. As the 50 Hz harmonics are present both at flat bottom and top energy, the tests where performed at injection. Due to a problem on the B2 RF, the MD started with a delay of 2.5 hours, allowing only for a 2.5 hour slot for the various tests. The MD consisted of two

Fills. For the first Fill (7342) a single bunch was injected in both beams in order to test the amplitude of the ADT excitations and the interlock of the IP1/5 phase knob. The filling scheme of the second Fill (7343) with three trains of 48 bunches in both beams is shown in Fig. 3. To achieve a constant sampling rate for the Fourier analysis of the bunch-by-bunch ADTObsBox data, the trains (blue) were symmetrically placed with a 120° azimuthal phase difference. Figure 4 illustrates the position of the three trains in the two beams. Based on

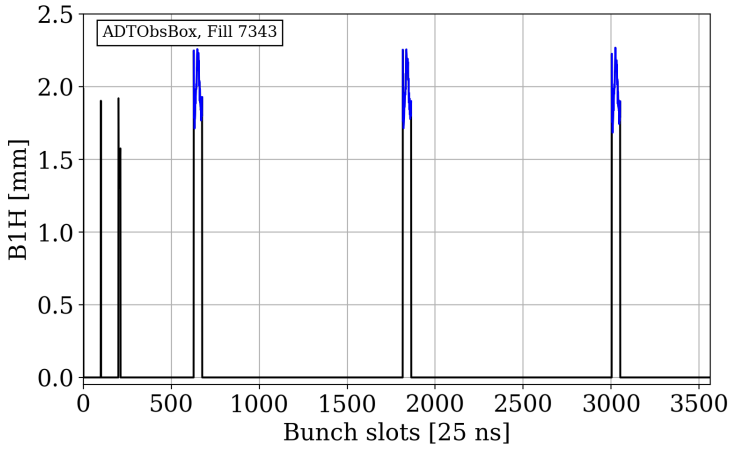

Figure 3: The filling scheme of the Fill 7343. The blue curve indicates the three trains of 48 bunches.

the filling scheme, the two beams encountered only in IP1 and 5.

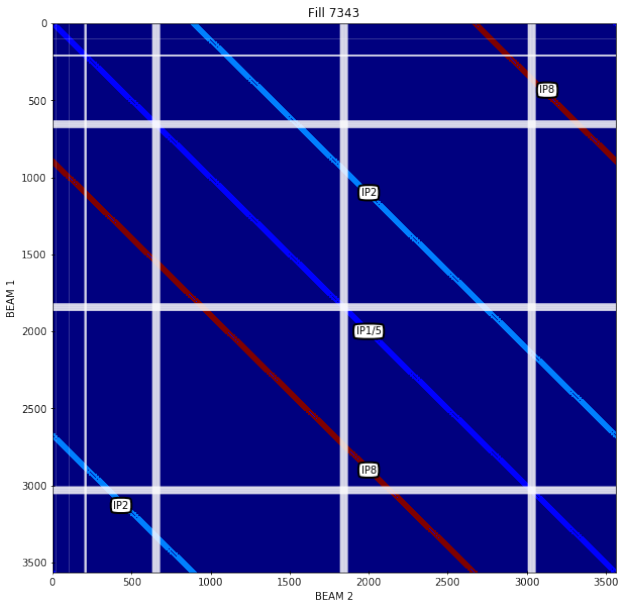

Figure 4: The encounters of the three trains (white lines) of the two Beams in Fill 7343.

The steps during the single-bunch Fill 7342 were the following:

- ADT external noise. B1H was excited with frequencies 0.6, 2.5 and 2.4 kHz. Then, an excitation at 2.4 kHz was individually applied to B1V, B2H and B2V.
- IP1/5 phase scan. A trim of +20° was applied to B1H. The trim quadrupole tolerances were exceeded, which resulted in a beam dump.

During this Fill, the ADTObsBox was acquiring data every minute for all beams and planes with the Q7, Q8, Q9 and Q10 pickups (not synchronized acquisition). Consecutive turn-by-turn data are also available from the MIM with a sampling rate equal to 16 times the revolution frequency (this reading is not bunch-by-bunch).

The steps during the Fill 7343 were the following:

- ADT external noise. B1H was excited with frequencies 2.4, 2.8, 3, 7.6, 8.8 and 8.1 kHz. An excitation at 3 kHz was applied to B2H.
- Active filters. The Active filters [10] of the eight sectors were disabled one-by-one. As a last step, all filters were switched off simultaneously.
- IP1/5 phase scan. A trim of ±8° was applied to all beams and planes separately.

During this Fill, consecutive high sampling rate data were collected for B1 with the MIM, as well as orbit and oscillation measurements with the DOROS pickups (not synchronized acquisition, J. Olexa). For this Fill, there are no regular acquisitions from the ADTObsBox and the stored measurements are based on the instability trigger. The time dedicated to each test for both Fills can be seen in Fig. 5.

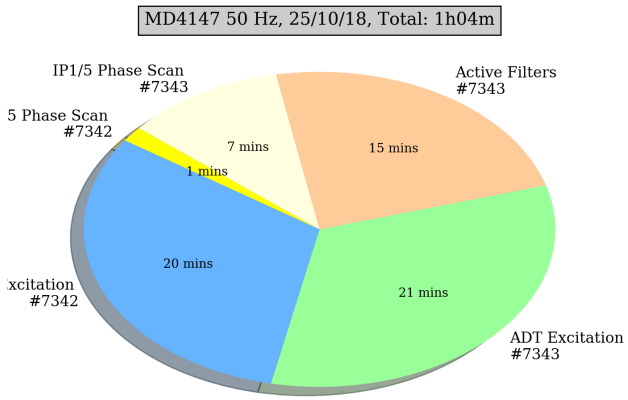

Figure 5: Breakdown of the MD4147's measurements.

3 High frequency cluster

Figure 6 depicts the horizontal spectrogram of Beam 1, as acquired from the MIM and centered around the low (left) and high (right) frequency cluster. In both cases, the modulation induced by the 50 Hz mains of the electrical network is observed. All harmonics

experience a modulation which is equal in frequency, synchronous in phase and an amplitude that is proportional to the order of the harmonic. The relationship between the order of the harmonic and the amplitude of the modulation indicates that both clusters emerge from a common origin.

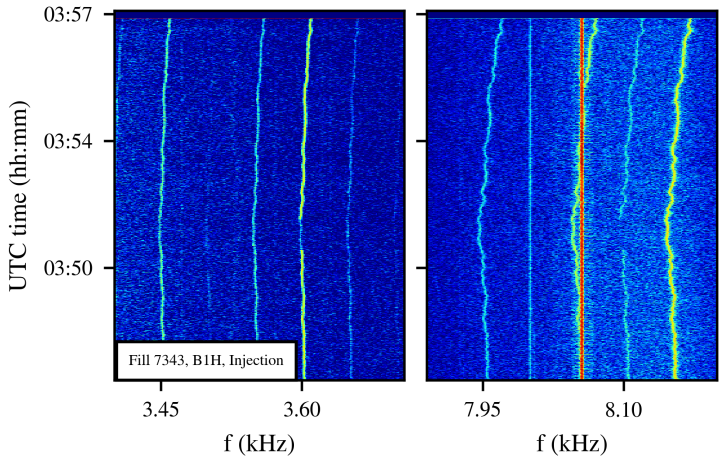

Figure 6: The horizontal spectrogram of Beam 1 centered around the low (left) and high (right) frequency cluster

To illustrate the common oscillation, an algorithm that can follow the evolution of each harmonics has been developed. The routine focuses around a regime in the vicinity of each harmonic and an precise determination of the frequency is achieved through the detection of the local maximum. Figure 7 shows the working principle of the algorithm (black curve) for a single harmonic.

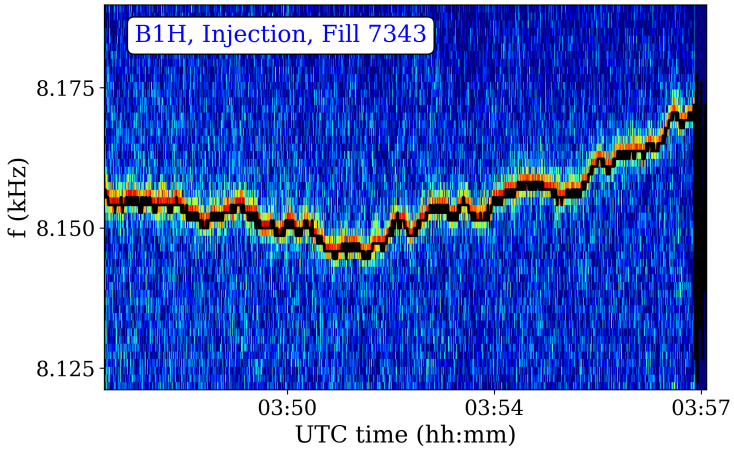

Figure 7: The horizontal spectrogram of Beam 1 centered around 8.15 kHz. The black curve represents the results of the frequency determination algorithm.

Figure 8 presents the voltage spectrogram of the power converter of the main dipoles in sector 1-2, centered around the low and high frequency cluster. The modulation from the 50 Hz mains is also visible in the harmonics of the power converter.

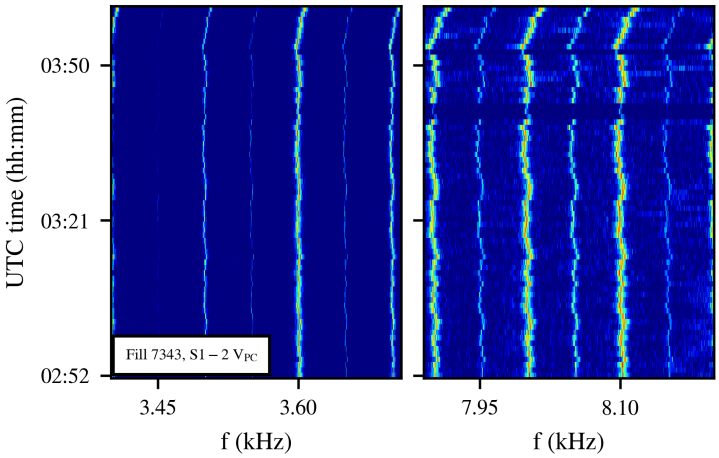

Figure 8: The voltage spectrum of the power converter of the main dipoles in sector 1-2, centered around the low (left) and high (right) frequency cluster.

As a next step, the aforementioned algorithm iterates over all the harmonics in the beam and the power converter spectrum. The frequency evolution of these spectral components, after normalizing with the order of the harmonic, is shown in Fig. 9 for the beam (black) and the power converter (blue). At approximately 6 a.m CET, a variation in frequency that exceeds the usual drift is observed in both spectra. The reproducibility of this effect at this time of the day has been validated with the analysis of measurements in different days and it appears to be the result of the changing power grid load at this time of the day.

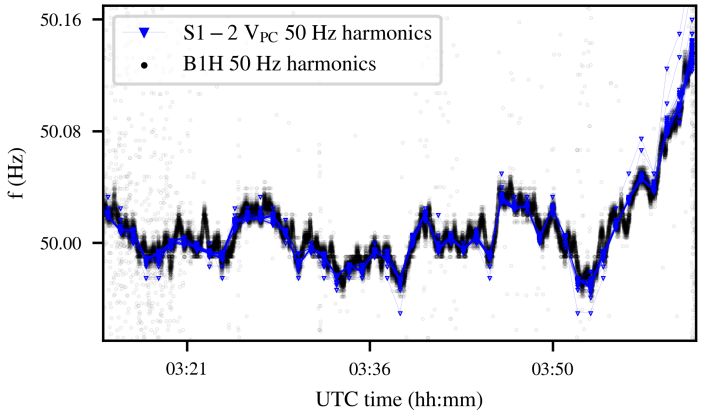

Figure 9: The common oscillation of the harmonics in the beam (black) and the power converter (blue), after normalising with the order of the harmonic.

Both clusters consist of multiple 50 Hz harmonics, the frequency of which varies due to the stability of the 50 Hz mains. This signature suggests that the origin of the harmonics is noise in thyristor commuted power converters, rather than Switch Mode.

A more detailed review of the spectrum reveals to existence of spectral components that are not affected by the stability of the 50 Hz mains. Figure 10 depicts the spectrogram

centered around 8.1 kHz. It can be seen that all the lines are modulated in frequency, apart from the 8, 8.05 and 8.32 kHz. In particular, for the case of the 8.05 kHz, the oscillating and the constant frequency components are superimposed. The fact that these frequencies are constant in time indicates that they are regular-clock frequencies, possibly arising from a Switch Mode power converter or from the clocks of the acquisition cards. It must be noted that these spectral components affect mostly the vertical plane and they are visible only at injection energy. Further studies are needed to determine if they result from a real beam excitation and to identify the origin.

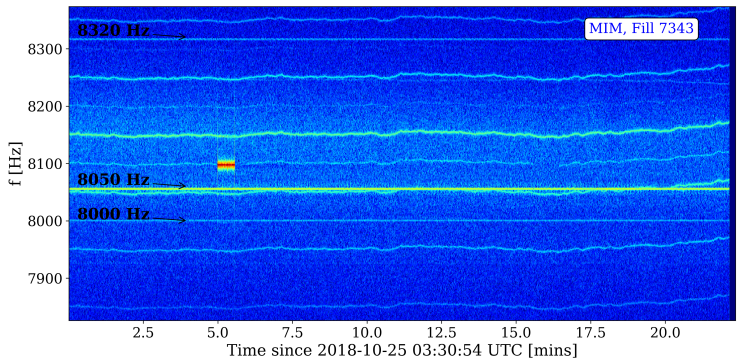

Figure 10: The constant frequency components in the horizontal spectrum of Beam 1 at injection.

4 Active Filters

To establish a correlation between the harmonics of the beam and the ones in the output of the power converters of the main dipoles, a modification in the configuration of the latter is needed. In this context, the eight Active filters were disabled sector-by-sector as shown in Fig. 11, were a color code is assigned to each sector. As a last step, the filters were switched off simultaneously.

Figure 12 illustrates the 3D spectrogram for the horizontal plane of Beam 1 during the Active filters tests. As a first step, the frequency range is limited around the h=12 harmonic. The blue line represents the amplitude evolution of the line i.e, the projection of its amplitude as a function of time. During these tests, abrupt changes in the amplitude evolution of the 600 Hz were observed.

Figure 13 presents the amplitude evolution of several harmonics in the low frequency cluster. The last curve corresponds to 3.6 kHz. The fact that the status of the Active filters has an impact on the spectrum of the beam provides evidence that the source of the low frequency cluster is noise in the power converters of the main bends. Based on this finding, all eight power converters contribute to this effect and the most impacted sector in terms of noise cannot be determined with the present information. It must be noted that these perturbations correspond to a maximum offset of $10^{-3}\sigma_{beam}$.

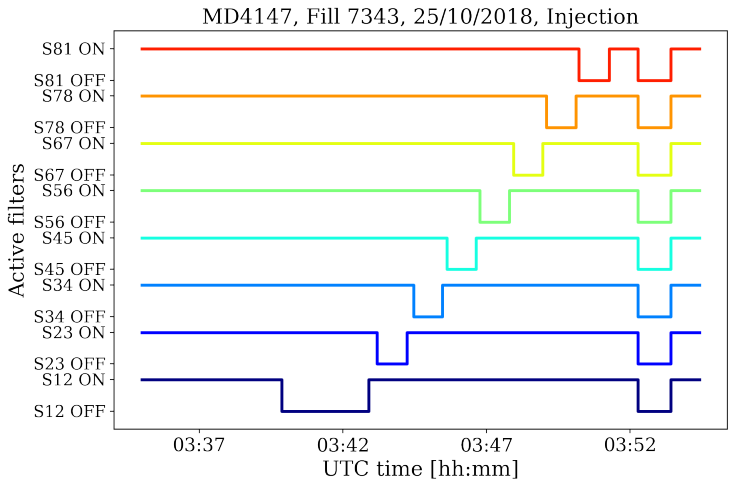

Figure 11: The status of the Active filters of the power converters of the main dipoles. A color code is assigned to each sector.

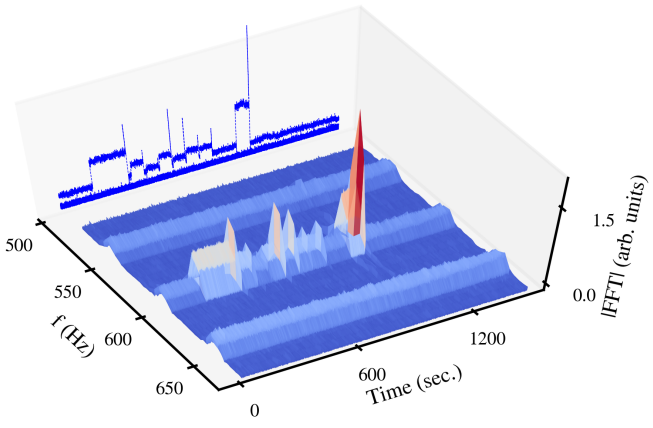

Figure 12: The 3D spectrogram of the horizontal plane of Beam 1, centered around the h=12 harmonic during the tests with the Active filters. The blue curve represents the amplitude evolution of the harmonic.

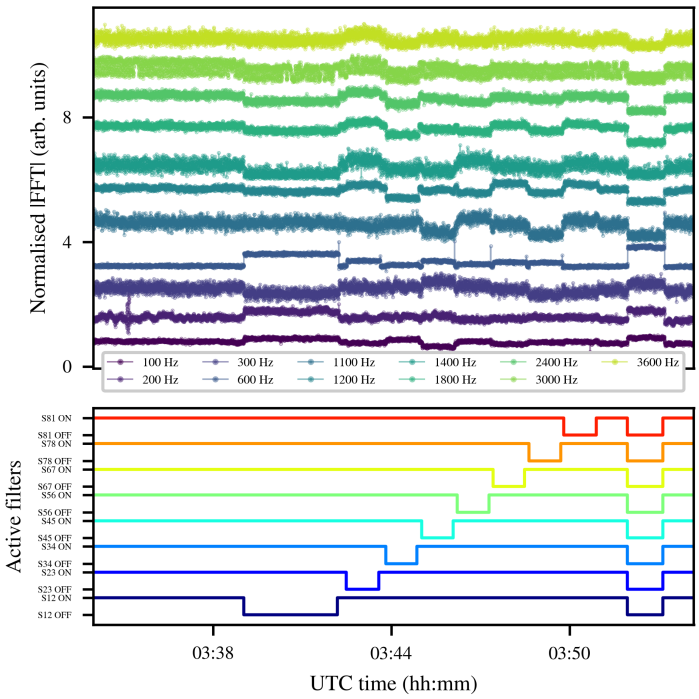

Figure 13: The amplitude evolution of the harmonics in the low frequency cluster (top) during the tests with the Active filters (bottom).

5 ADT excitations

5.1 Benchmark of noise simulations

The ADT was used to apply controlled dipolar excitations on the beam. Some of the excitations led to a significant reduction of the beam lifetime. Figure 14 presents the HS BBQ spectrogram for the horizontal (left) and vertical (right) plane of Beam 1 (top) and 2 (middle) in the single-bunch Fill 7342. The evolution of the lifetime during these excitations is shown with the blue and red curve for Beam 1 and 2, respectively. The horizontal excitations performed in the second Fill with trains are also shown (bottom).

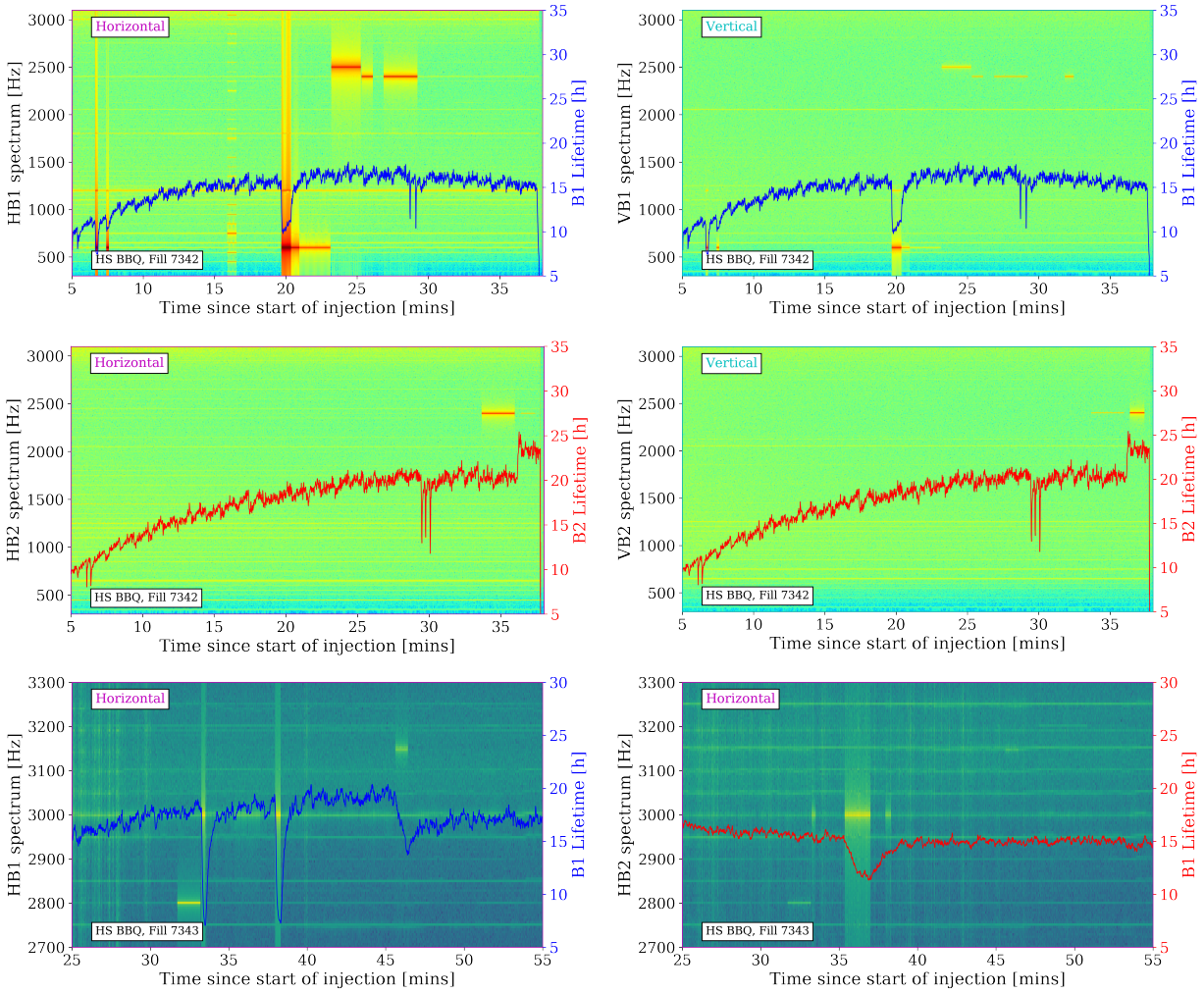

Figure 14: HS BBQ spectrograms and the lifetime of Beam 1 (blue) and 2 (red) during the ADT excitations in the Fill 7342 (two top) and 7343 (bottom).

To retrieve the initial deflection applied from the transverse damper kickers, the offset and the frequency are extracted from the calibrated ADTObsBox beam spectrum. Figure 15 presents the spectrum during an excitation at 2.5 kHz. The green marker indicates the offset observed on the beam. Then, based on these two parameters, the equivalent kick at the location of one of the ADT kickers is computed (see Appendix A).

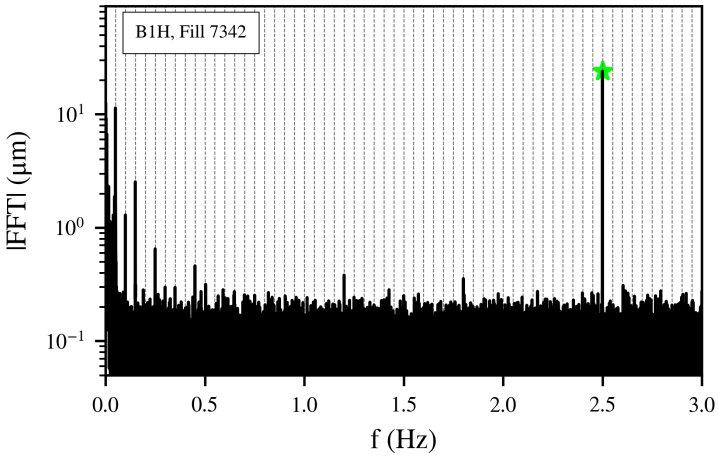

Figure 15: The horizontal spectrum of Beam 1 during an excitation at 2.5 kHz in the Fill 7342.

These excitations are used to validate the 6D single-particle simulations including noise [11, 12]. In particular, a distribution of particles is tracked in the LHC lattice at injection for 10^6 turns. The initial conditions form a polar grid in the configuration space with nine angles and a radius from from two to ten σ with a step of two σ. In the longitudinal plane, the momentum deviation of the particles is equal to 3/4 of the bucket height. The excitation is simulated by including a modulated dipole at the location of one of the ADT kickers with the DYNK module of SixTrack [13]. The observation point is defined at the location of the Q7 pickup. For each study, a different combination of frequency and amplitude of the noise is selected. Figure 16 presents the deflection as a function of the excitation frequency and a color-code is assigned to the minimum DA. In this way, the regime where the noise impacts the DA is identified. The equivalent defections, as computed from the beam spectrum, are shown with the star-shaped markers. The excitations that led to a reduction of lifetime are shown with red, while the ones that had no impact are shown with blue. A comparison between the simulations and the kicks computed from the beam spectrum suggests that there is a good agreement between the two for the majority of the frequencies.

It must be noted however, that the equivalent kick from an excitation at 600 Hz, as computed from the beam spectrum, corresponds to a deflection that exceeds the maximum ADT kick strength (2 μrad at injection). Furthermore, a comparison between the equivalent (from the spectrum) and the maximum kick computed from the ADT parameters (from D. Valuch) reveals that there is an important discrepancy between the two for all the excitations. Figure 17 (left) presents the kicks computed from the ADT parameters (star shaped markers) and from the beam spectrum (square shaped markers). The offsets computed from the beam spectrum and the ADT parameters are shown in Fig. 17 (left). A discrepancy is found between the two by a factor of approximately 100. In particular, the offset observed in the beam spectrum is more important than the one expected based on the maximum value of the deflection. To identify the origin of this discrepancy further experiments are needed, however the present hypothesis is that there is an interplay between the excitations at multiples of 50 Hz and the harmonics that are present in the spectrum due to noise.

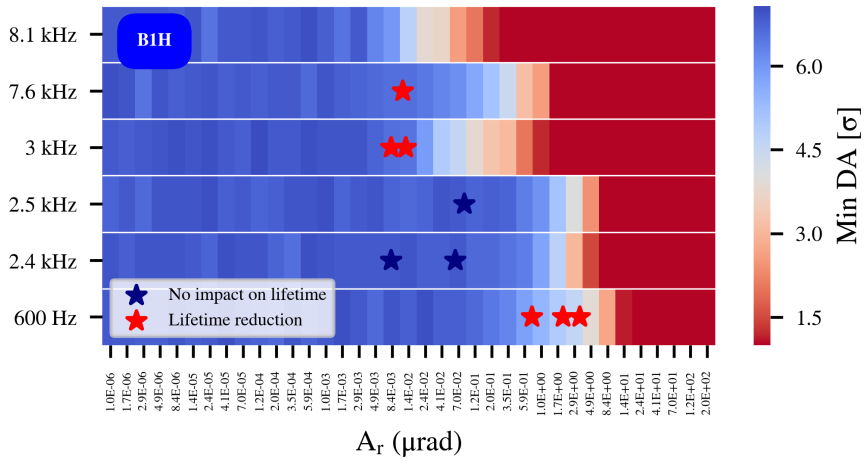

Figure 16: The excitation amplitude as a function of the frequency. A color code is assigned to the minimum DA. The star shaped markers indicate the excitations performed during the MD, during which a lifetime reduction was (red) or was not (blue) observed.

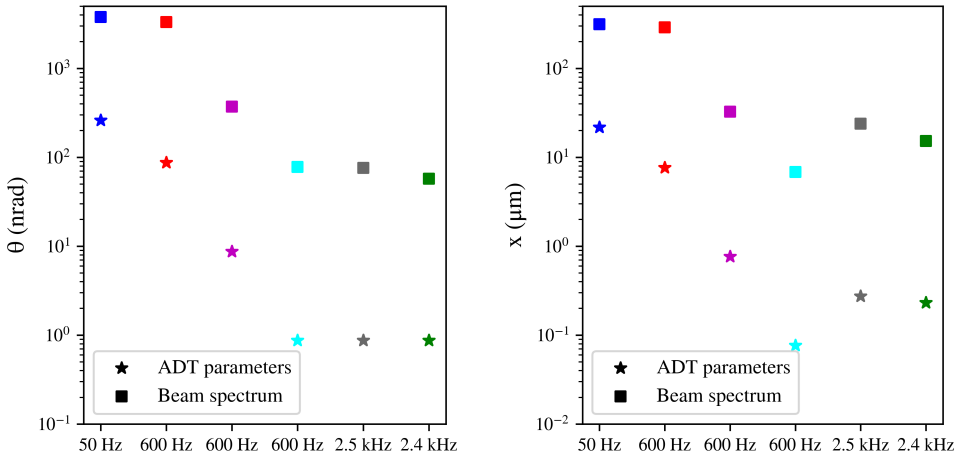

Figure 17: The kicks (left) and offsets (right) computed from the beam spectrum (square markers) and the ADT parameters (star markers), respectively, as a function of the excitation frequency.

Furthermore, both in simulations and experimental observations, a strong dipolar excitation at a frequency outside the range of the betatron tune spread leads to a reduction of lifetime. This is due to the combination of a dipolar modulation and the non-linear elements in the lattice, which result, through feed-down, to a tune modulation. Figure 18 shows the frequency maps [14–16] at injection in the absence of noise (first) and in the presence of dipolar noise at 600 Hz for two values of the amplitude (second and third). Additional resonances are excited in the form of sidebands (red) that indicate the existence of a tune modulation, which eventually leads to proton losses.

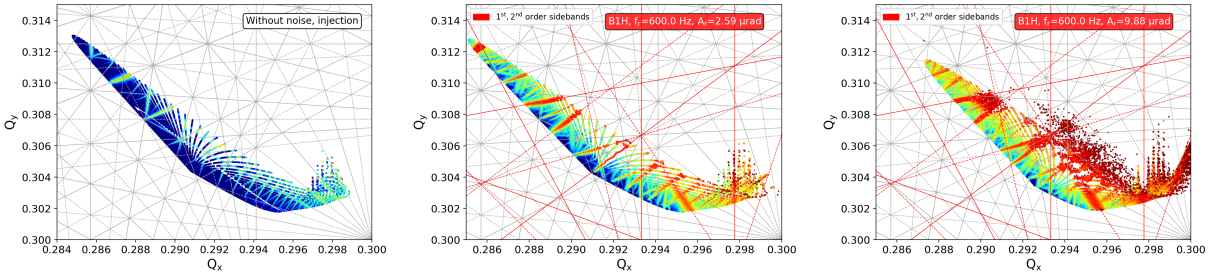

Figure 18: Frequency Map Analysis at injection without noise (first) and after injecting a dipolar excitation at 600 Hz for two values of the deflection (second and last). The gray and red lines represent the regular and side band resonances respectively.

5.2 Horizontal/vertical coupling

The 50 Hz harmonics are an effect which mainly affects the horizontal plane. However, the harmonics are also present in the vertical plane. To determine whether this is the result of the machine coupling, a controlled excitation was applied only in the horizontal plane of Beam 1. Figure 19 shows the spectrum of the horizontal (magenta) and vertical plane (cyan) at the time span of the excitation. The excitation at 600 Hz is visible in both planes. After the normalization of the spectra with the β-functions of the corresponding pickups, the comparison between the two planes yields a factor of 1.6% at injection energy. This observation shows that noise injected in the horizontal plane, such as the 50 Hz harmonics from the dipoles, is expected to be present also in the vertical plane through coupling.

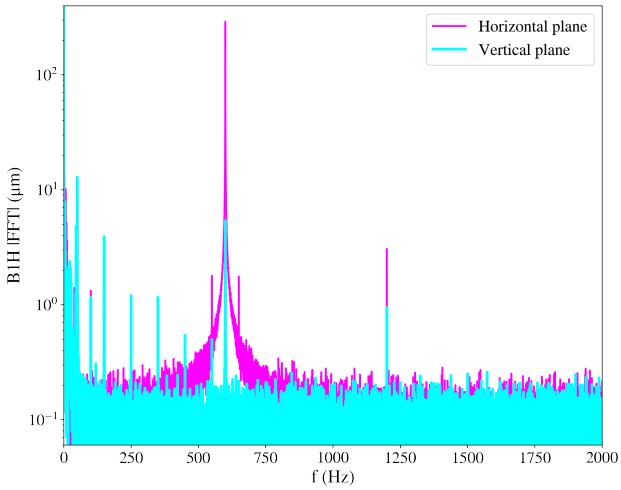

Figure 19: The spectrum of Beam 1 in the horizontal (magenta) and vertical (cyan) plane during an excitation in the horizontal plane.

5.3 Bunch-by-bunch variations

From the bunch-by-bunch acquisitions of the ADTObsBox, the spectrum of each bunch is computed during several controlled excitations. As the amplitudes of the excitations

exceeded the noise threshold of the single-bunch spectrum, the offset and the phase of the excitations are determined bunch-by-bunch. Figure 20 shows the offset (left) and the phase (right) as a function of the bunch position in the ring during an excitation at 2.8 kHz. A color code is assigned to the bunch number. The amplitude of the 2.8 kHz spectral line is approximately constant between the bunches. The phase determination shows that the dephasing of the injected noise is linearly proportional to the frequency and the time delay of the trailing bunches from the first one in the machine, which is considered as the reference (black dashed line).

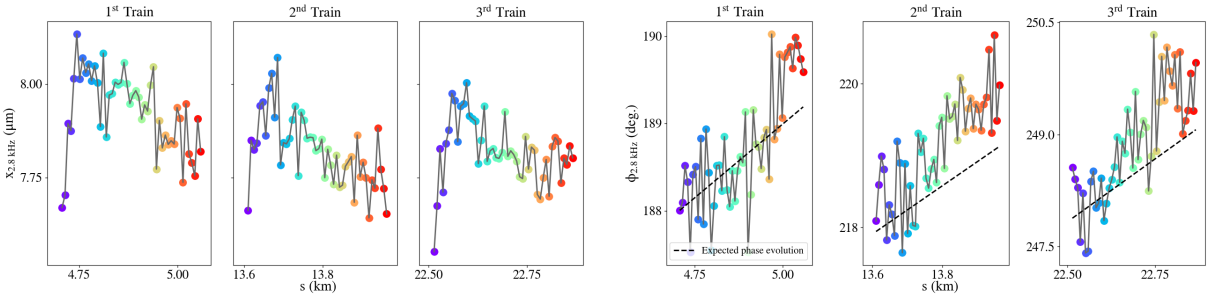

Figure 20: The bunch-by-bunch amplitude (left) and phase (right) evolution of an excitation at 2.8 kHz as computed from the spectrum. The vertical dashed line illustrates the expected phase evolution across the trains and a color code is assigned to the different bunches.

However, bunch-by-bunch variations are observed both in terms of amplitude and phase when significant deflections were applied. Figure 21 depicts the offset and the phase as a function of the bunch positions during an excitation at 3 kHz with an average offset of 23.9 μm. In this case, the amplitude across the bunches is not constant and a discrepancy of a few degrees is observed in the phase evolution from the one expected. The mechanism that leads to these variations is not yet identified.

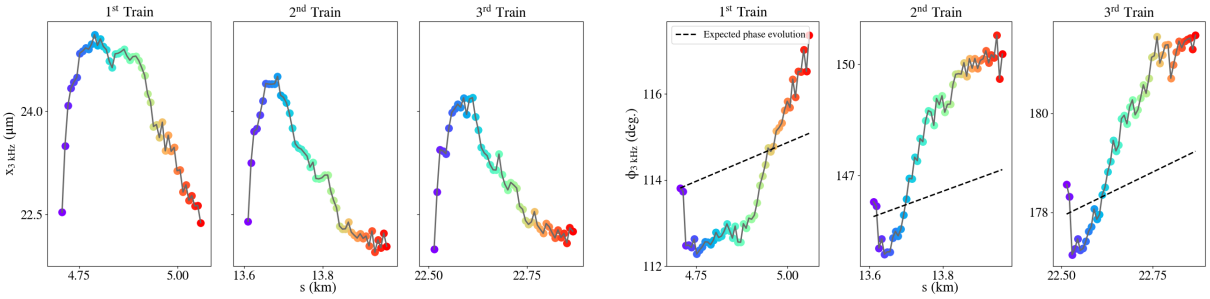

Figure 21: The bunch-by-bunch amplitude (left) and phase (right) evolution of an excitation at 3 kHz as computed from the spectrum. The vertical dashed line illustrates the expected phase evolution across the trains and a color code is assigned to the different bunches.

5.4 Beam 1/2 coupling

An additional observation is that, in the presence of trains, a coupling of the noise between the two beams is observed. Figure 22 shows the HS BBQ spectrogram of Beam 1 (left)

and 2 (right) during several excitations that were individually applied to each beam. These excitations are visible in both spectra, an effect that was not observed in the single-bunch Fill. To further investigate this effect, the bunch-by-bunch amplitude of the injected noise, which was only applied in Beam 1, is computed for both beams. From Fig. 23 it can be seen that the excitation is also visible in Beam 2 with an amplitude that is maximum at the center of the trains. These patterns are consistent with the long-range encounters that maximize at the center of the trains. From this observations it is concluded that there is a coupling of the injected noise between the two beams through beam-beam effects.

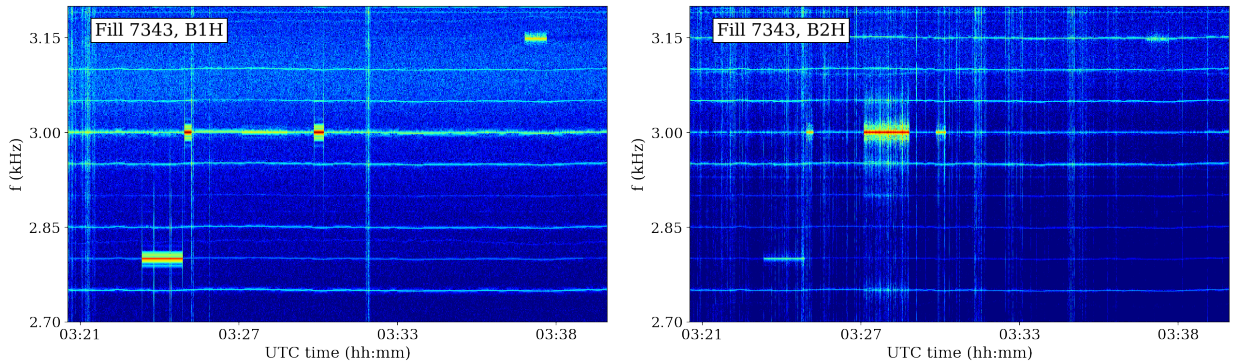

Figure 22: The HS BBQ spectrogram of Beam 1 (left) and 2 (left) during the controlled excitations.

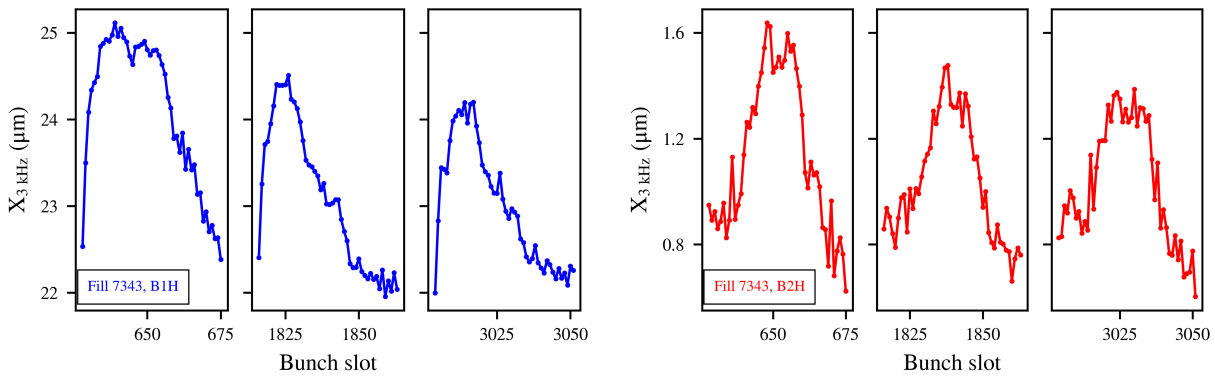

Figure 23: The bunch-by-bunch amplitude evolution of an excitation at 3 kHz, which was only applied to Beam 1, as computed from the beam spectrum for Beam 1 (left) and 2 (right)

6 IP1/5 phase scan

The aim of this test is to reproduce the results of Fig. 2 at injection. During the first, single-bunch Fill, the phase knob that allows the control of the betatronic phase advance between IP1/IP5 and IP5/IP1, while keeping the tune constant, was employed. A trim of 20° was applied to B1H, which lead to a beam dump, due to the interlock in the current of the trim quadrupoles' PCs.

In the second Fill, a trim was applied for both beams and planes in a range of ±8 ° instead of ±20 °, in order to avoid a beam dump. Figure 24 shows the impact of the horizontal (cyan) and vertical (magenta) trims on the lifetime of Beam 1 (blue) and 2 (red). The dashed line represents the initial lifetime, prior to the application of the phase trims. In this case, a lifetime variation is visible, an effect which was not observed during similar tests at top energy.

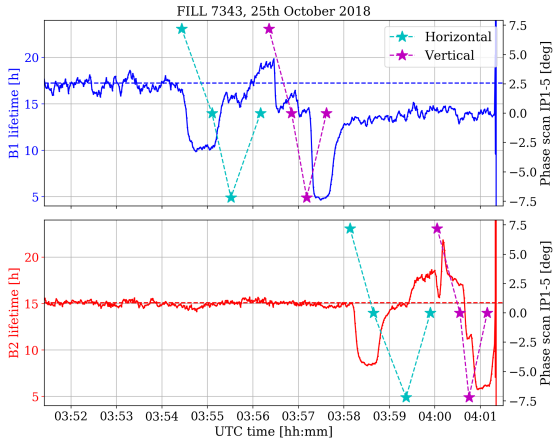

Figure 24: Lifetime during the horizontal (cyan) and vertical (magenta) IP1/5 phase trim for B1 (blue) and B2 (red).

Figure 25 depicts the evolution of two 50 Hz harmonics during the trims. No impact is observed in their amplitude evolution and the results of Fig. 2 were not reproduced. It is concluded that the lifetime variation is not correlated with changes in the 50 Hz harmonics. The cause behind this lifetime changes still needs to be understood.

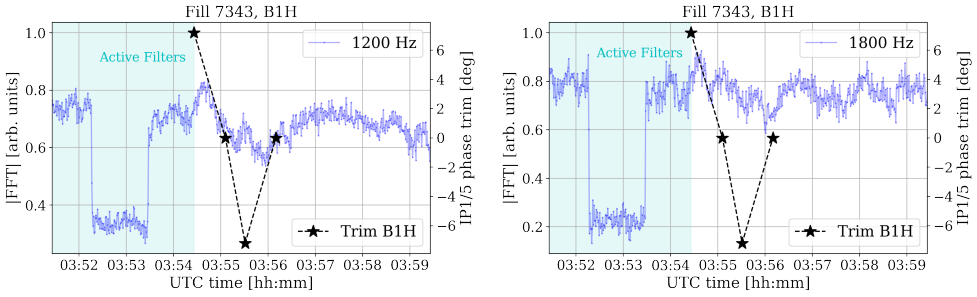

Figure 25: B1H amplitude evolution of 1.2 (left) and 1.8 kHz (right) during the B1H IP1/5 phase trims.

7 Conclusions

Although the MD duration was limited to 2.5 h, a large amount of information were collected concerning the 50 Hz harmonics, through systematic high-sampling rate measurements, and the impact of controlled dipolar excitations on the beam.

First, a similar signature between the harmonics of the low and high frequency cluster is reported. Both clusters consist of multiple 50 Hz harmonics that experience a modulation arising from the stability of the 50 Hz mains, which propagates to all the harmonics with an amplitude that is proportional to the order of the harmonic. This observation suggests that both clusters emerge from a common source. The similar signature between the two was found thanks to the high-sampling rate and consecutive measurements from the MIM.

Second, through the tests with the Active Filters of the main dipole power converters, the correlation between the harmonics of the low frequency cluster (up to 3.6 kHz) in the beam and the power converters was also verified at injection energy. From this observations it is concluded that all eight sectors contribute to this effect.

From the controlled ADT excitations, a good agreement is found between the predictions of the DA simulations in the presence of dipolar noise and the impact on the beam lifetime that was observed experimentally. However, an important discrepancy is found between the expected and the observed offsets on the beam spectrum during the excitations, an effect that needs to be further understood. In particular, it was observed that during the excitations at a harmonics of 50 Hz, a larger offset was observed in the beam spectrum than the one expected by a factor of approximately 100. Experimentally, it was confirmed that a horizontal excitation is also affecting the vertical plane through the coupling of the machine. Furthermore, it was demonstrated that, in the presence of trains, the noise can couple between the two beams through beam-beam effects. Finally, further studies are required to identify the mechanism that leads to the bunch-by-bunch variations of the injected noise in the presence of strong dipolar excitations ($> 20\mu$m).

Acknowledgements

We are grateful to all the support received from the Machine Protection Panel, LHC-OP team, the LHC MD coordinators and the Electrical Power Converters Group.

A Linear formalism of a modulated dipolar field error

A modulated dipolar field error Θ_p with a deflection θ_p and a frequency of $\mathrm{Q_p}$ oscillations per turn can be represented as:

$$\bar{P}_n = \begin{pmatrix} 0 \\ \Theta_p(n) \end{pmatrix} = \begin{pmatrix} 0 \\ \theta_p \cos\left(2\pi Q_p n\right) \end{pmatrix} \tag{1}$$

where n is the turn considered. In normalized coordinates and in linear approximation:

$$\bar{X}_N = M^N \bar{X}_0 + \sum_{n=1}^{N} M^{N-n} \bar{P}_n \tag{2}$$

where $\bar{X}_0$, $\bar{X}_N$ is the matrix representation of the position and momentum initially and a turn N, respectively and M is the linear rotation with:

$$M^N = \begin{pmatrix} \cos(2\pi QN) & \sin(2\pi QN) \\ -\sin(2\pi QN) & \cos(2\pi QN) \end{pmatrix} \tag{3}$$

where Q is the betatron tune. Combining Eq. (1), (2) and (3) yields:

$$\Delta x(N) = \sum_{n=-\infty}^{N} \Theta_p(n) \sin\left(2(N-n)\pi Q\right) \tag{4}$$

Combining Eq. (1) and (4), the closed form expression is:

$$\Delta x(N) = \frac{\theta_p \cos\left(2\pi N Q_p\right) \sin\left(2\pi Q\right)}{2\left(\cos\left(2\pi Q_p\right) - \cos(2\pi Q)\right)} \tag{5}$$

In physical coordinates, the maximum offset at a location with β from a kick at β_s is:

$$|\Delta x| = \left| \frac{\sqrt{\beta_s \beta}\theta_p \sin\left(2\pi Q\right)}{2\left(\cos\left(2\pi Q_p\right) - \cos(2\pi Q)\right)} \right| \tag{6}$$

References

[1] G. Arduini. (5th Aug. 2015). 50 hz lines studies: First observations, LHC Machine Committee, CERN, [Online]. Available: https://indico.cern.ch/event/436679/contributions/1085928/attachments/1136594/1627012/LMC05082015_50Hz_04082015.pdf.

[2] R. De Maria, *Observation of 50hz lines in the lhc bbq system*, LHC Beam Operation Committee, 16th Oct. 2012. [Online]. Available: https://lhc-beam-operation-committee.web.cern.ch/lhc-beam-operation-committee/minutes/Meeting51-16_10_2012/workoutline.pdf.

[3] S. Kostoglou, *Status of noise studies in the lhc and expected impact for the hl-lhc*, WP2, 26th Nov. 2019. [Online]. Available: https://indico.cern.ch/event/860231/contributions/3622905/attachments/1951138/3239075/WP2_26_11_2019_noise.pdf.

[4] G. Sterbini, *Latest on noise effects on the beam*, HL-LHC Collaboration Meeting, 15th Oct. 2019. [Online]. Available: https://indico.cern.ch/event/806637/contributions/3573640/attachments/1926694/3190058/HL_LHC_2019_sterbini.pdf.

[5] S. Kostoglou, *Sources of noise: 50 hz harmonics on the beam spectrum*, LHC Machine Committee, CERN, 4th Dec. 2019. [Online]. Available: https://indico.cern.ch/event/868659/contributions/3661618/attachments/1956282/3249703/LMC_50Hz_04122019.pdf.

[6] T. Levens, T. Lefèvre and D. Valuch, "Initial results from the lhc multi-band instability monitor", in *Int. Beam Instrumentation Conf.(IBIC'18), Shanghai, China, 09-13 September 2018*, JACOW Publishing, Geneva, Switzerland, 2019, pp. 314–318.

[7] L. Carver, X. Buffat, A. Butterworth, W. Höfle, G. Iadarola, G. Kotzian, K. Li, E. Métral, M. Ojeda Sandonís, M. Söderén and D. Valuch, "Usage of the Transverse Damper Observation Box for High Sampling Rate Transverse Position Data in the LHC", no. CERN-ACC-2017-117, MOPAB113. 4 p, 2017. DOI: 10.18429/JACoW-IPAC2017-MOPAB113. [Online]. Available: https://cds.cern.ch/record/2289712.

[8] N. Karastathis. (11th Sep. 2018). Md3583: Beam-beam long range 2018, LHC Studies Working Group, CERN, [Online]. Available: https://lhc-beam-operation-committee.web.cern.ch/lhc-beam-operation-committee/minutes/Meeting51-16_10_2012/workoutline.pdf.

[9] (25th Oct. 2018). Md4147 procedure, [Online]. Available: https://asm.cern.ch/md/requests/LHC/4147?query=%5C%2522Created%5C%2520by%5C%2522%5C%2520%5C%253D%5C%2520%5C%2522Sofia%5C%2520Kostoglou%5C%2522&mode=d.

[10] A. Verweij, R. Schmidt, M. Gruwé, V. Parma, H. Thiessen, S. Fehér, M. Zerlauth, R. Denz, L. Ponce, V. Kain *et al.*, "Performance of the main dipole magnet circuits of the lhc during commissioning", Tech. Rep., 2008.

[11] Sixtrack. (), [Online]. Available: http://sixtrack.web.cern.ch/SixTrack/.

[12] R. D. Maria, J. Andersson, V. K. B. Olsen, L. Field, M. Giovannozzi, P. D. Hermes, N. Høimyr, S. Kostoglou, G. Iadarola, E. Mcintosh, A. Mereghetti, J. W. Molson, D. Pellegrini, T. Persson, M. Schwinzerl, E. H. Maclean, K. Sjobak, I. Zacharov and S. Singh, "SixTrack project: Status, runtime environment, and new developments", in *Proceedings, 13th International Computational Accelerator Physics Conference, ICAP2018: Key West, FL, USA, 20-24 October 2018*, 2019, TUPAF02. DOI: 10.18429/JACoW-ICAP2018-TUPAF02.

[13] K. Sjobak, V. K. B. Olsen, R. D. Maria, M. Fitterer, A. S. García, H. Garcia-Morales, A. Mereghetti, J. F. Wagner and S. J. Wretborn, *Dynamic simulations in sixtrack*, 2018. arXiv: 1808.06248 [physics.acc-ph].

[14] Y. Papaphilippou, "Detecting chaos in particle accelerators through the frequency map analysis method", *Chaos: An Interdisciplinary Journal of Nonlinear Science*, vol. 24, no. 2, p. 024 412, 2014.

[15] J. Laskar, "Introduction to frequency map analysis", in *Hamiltonian systems with three or more degrees of freedom*, Springer, 1999, pp. 134–150.

[16] J. Laskar, "Frequency map analysis and particle accelerators", in *Proceedings of the 2003 Particle Accelerator Conference*, IEEE, vol. 1, 2003, pp. 378–382.